Performance of Algorithms for Retrieving Chlorophyll a Concentrations in the Arctic Ocean: Impact on Primary Production Estimates

Juan Li , Atsushi Matsuoka , Xiaoping Pang * , Philippe Massicotte , Marcel Babin

Posted Date: 25 December 2023

doi: 10.20944/preprints202312.1775.v1

Keywords: Arctic Ocean; chlorophyll a algorithm; colored and detrital material; primary production

Article

Performance of Algorithms for Retrieving Chlorophyll *a* Concentrations in the Arctic Ocean: Impact on Primary Production Estimates

Juan Li [1,2,3], Atsushi Matsuoka [4], Xiaoping Pang [1,3,*], Phillipe Massicotte [2] and Marcel Babin [2]

[1] Chinese Antarctic Center of Surveying and Mapping, Wuhan University, Wuhan 430079, China
[2] Takuvik Joint International Laboratory, CNRS (France) & ULaval (Canada), Pavillon Alexandre-Vachon, Local 2064, 1045, avenue de la Médecine, Département de Biologie, Université Laval, Québec, QC G1V 0A6, Canada
[3] Key Laboratory of Polar Environment Monitoring and Public Governance (Wuhan University), Ministry of Education, Wuhan 430079, China
[4] University of New Hampshire, Durham, Institute for the Study of Earth, Oceans, and Space, Durham, New Hampshire 03824, USA
* Correspondence: pxp@whu.edu.cn

Abstract: Chlorophyll *a* concentration (Chl) is a key variable for estimating primary production (PP) through ocean-color remote sensing (OCRS). Accurate Chl estimates are crucial for better understanding of the spatio-temporal trends of PP in recent decades as a consequence of climate change. However, a number of studies have reported that currently operational chlorophyll *a* algorithms perform poorly in the Arctic Ocean (AO), largely due to the interference of colored and detrital material (CDM) with the phytoplankton signal in the visible part of the spectrum. To determine how and to what extent CDM biases the estimation of Chl, we evaluated the performances of 8 currently available ocean-color algorithms: OC4v6, OC3Mv6, OC3V, OC4L, OC4P, AO.emp, GSM01 and AO.GSM. Our results suggest that the empirical AO.emp algorithm performs the best overall, but for waters with high CDM ($a_{cdm}(443) > 0.067$ m^{-1}), a common scenario in the Arctic, the two semi-analytical GSM models yield better performance. In addition, sensitivity analyses using a spectrally- and vertically-resolved Arctic primary-production model show that errors in Chl estimates mostly propagate proportionally to PP estimates, with amplification of up to 7%. We also demonstrate that the higher the level of CDM in relation to Chl in the water column, the larger the bias in both Chl and PP estimates. Lastly, although the AO.GSM is the best overall performer among the algorithms tested, it tends to fail for a significant number of pixels (16.2% according to the present study), particularly for waters with high CDM. Our results therefore suggest the ongoing need to develop an algorithm that provides reasonable Chl estimates for a wide range of optically-complex Arctic waters.

Keywords: Arctic Ocean; chlorophyll *a* algorithm; colored and detrital material; primary production

1. Introduction

The Arctic Ocean (AO) is the ocean that receives the largest amount of river discharge relative to its volume (11% of global river discharge while its volume represents only 1% of global ocean, [1]). In this context, as its drainage basin is even larger than its area, the AO is characterized by a high level of colored dissolved organic matter (CDOM) in relation to other optically significant components when compared to other oceans. In addition, under the pressure of global warming, significant amounts of dissolved organic carbon (DOC) deriving from the thawing of permafrost are delivered into the AO, currently experiencing a long-term increase in river discharge [2,3]. As a result,

 doi:10.20944/preprints202312.1775.v1

unlike other oceans, the optical properties of the AO are much affected by CDOM, as pointed out by multiple studies [4–11].

In this most river-influenced and landlocked of oceans [12], the impact of CDOM on optical properties is most prominent in Arctic coastal regions, especially in and around large river plumes, and under the influence of coastal erosion, permafrost thaw and glacial run-off. In such complex coastal waters, phytoplankton blooms are a common major ecological event making up a substantial part of the annual primary production and energy transfer supporting the entire marine food web [13,14].

Ocean-color remote sensing (OCRS) has been used extensively to estimate primary production in the AO (e.g. [15],[16],[17],[18]). Despite the efforts made to address the complex optical properties using regionally tuned empirical [19] or semi-analytical algorithms (e.g. [18]), doubts persist regarding the validity of the very high PP values systematically found in coastal waters, especially above the Russian continental shelves. More specifically, uncertainty surrounding chlorophyll a concentration (Chl) retrievals, and consequently PP estimates, is not quantitatively known.

CDOM exhibits high absorption in the ultraviolet and visible portion of the spectrum, and decays approximately exponentially to the red [20]. Waters with high CDOM content (denoted as "CDOM-rich waters" hereafter) are subject to significant interference with the phytoplankton signal in the blue-to-green band ratio for derivations of Chl. Algorithms for the latter are not limited to global empirical algorithms (distinguished by the number of wavelengths, the satellite involved, and the version number; e.g. OC4v6, OC3Mv6, and OC4Mev6; [21],[22]), but also include Arctic regional algorithms (e.g. OC4L and OC4P [19,23] respectively) and the semi-analytical algorithm GSM01 (Garver-Seigel-Maritorena algorithm [24]).

Before seeking solutions to the problems that high CDOM content in the water column raise for obtaining accurate Chl estimates, we first need to assess how and to what extent CDOM biases Chl estimates. In addition, Chl being a key variable used for PP estimates, it is necessary to quantify uncertainties in PP estimates induced by errors in algorithm-derived Chl estimates. Unlike the case of oligotrophic waters where large relative errors in Chl estimates have limited impact on absolute PP estimates, for coastal eutrophic waters, small relative errors in Chl estimates can result in significant absolute errors in the estimation of PP.

To address these issues, we first built a high-quality bio-optical *in situ* dataset at a pan-Arctic scale. The objectives of this study were then to: 1) evaluate the performances of currently available ocean-color algorithms in terms of the impact of colored and detrital material (CDM); and 2) determine how errors in algorithm-derived Chl propagate to PP estimates using a spectrally- and vertically-resolved Arctic primary-production model. Here, CDM (sum of CDOM and non-algal particles) was used instead of CDOM as CDM is a direct retrieval from OCRS, and the absorption due to non-algal particles (NAP) is limited compared to CDOM.

2. Data

2.1. In situ data

The Arctic dataset that we used to evaluate the algorithms was gathered from the following five cruises: the France-Canada-USA joint Arctic campaign MALINA [25], ICESCAPE (Impacts of Climate on Ecosystems and Chemistry of the Arctic Pacific Environment) 2010 and 2011 [26], Tara Oceans Polar Circle expedition [27], and the GREEN EDGE project [28]. Sampling of MALINA and GREEN EDGE (ship operation) was conducted aboard the Canadian icebreaker *CCGS Amundsen*. The two ICESCAPEs were aboard the US icebreaker *USCGC Healy*. The Tara expedition was conducted using the French schooner *TARA*.

Among the measured variables, remote-sensing reflectance $R_{rs}(\lambda)$ and Chl are the two most important variables for evaluating the performance of Chl algorithms. In the present study, all $R_{rs}(\lambda)$ values were determined with the same instrument, the Compact-Optical Profiling System (C-OPS, Biospherical Instrument Inc.). Specific information about the C-OPS is provided by [29]. Briefly, the C-OPS consists of two 7 cm-diameter radiometers: one measuring in-water upwelling radiance

Preprints (www.preprints.org) | NOT PEER-REVIEWED | Posted: 25 December 2023 doi:10.20944/preprints202312.1775.v1

$L_u(\lambda, z)$ and the other measuring in-water downward irradiance $E_d(\lambda, z)$, pressure/depth, and dual axes tilts. The above-water downward solar irradiance ($E_s(\lambda)$) was also measured to account for changes in the incident light field during in-water profiles. All radiometers were equipped with 19 state-of-the-art microradiometers spanning the 320–780 nm spectral range, and only data with tilt angles less than 5° were used. Subsurface $L_u^-(\lambda)$ and $E_d^-(\lambda)$ were derived by loess extrapolating $L_u(\lambda, z)$ and $E_d(\lambda)$ through progressively optimized depth intervals within the first optical depth [30]. Finally, $R_{rs}(\lambda)$ was calculated as: $R_{rs}(\lambda) = 0.52L_u^-(\lambda)/E_d^-(\lambda)$. Only wavebands common to the five selected cruises (412, 443, 490, 510, 555 and 670 nm) were used in this study.

Chl was determined by High-Performance Liquid Chromatography (HPLC). Generally, 25 mm GF/F filters were used to collect phytoplankton from seawater samples. Filters were extracted in 100% methanol, disrupted by sonication and clarified by filtration (GF/F Whatman) before being analyzed by HPLC later in the laboratory to obtain separated pigments. HPLC measurements for ICESCAPE samples followed the protocols described in [31], while for MALINA, Tara-Arctic, and GREEN EDGE samples, we applied a protocol modified from [32] to increase sensitivity in the analysis of ultra-oligotrophic waters. Finally, total chlorophyll a pigment concentration was defined as the sum of mono and divinyl chlorophyll a concentrations, chlorophyllide a and the allomeric and epimeric forms of chlorophyll a [33,34].

The absorption coefficient of CDM ($a_{cdm}(\lambda)$) is the sum of the absorption coefficients of CDOM ($a_{cdom}(\lambda)$) and NAP ($a_{nap}(\lambda)$). $a_{cdom}(\lambda)$ was measured using a liquid-core waveguide system, UltraPath (WPIInc.,http://www.wpi-europe.com/products/spectroscopy/ultrapath.htm) following [35] and [7]. $a_{nap}(\lambda)$ was determined using a Perkin-Elmer Lambda-19 spectrophotometer equipped with a 15 cm integrating sphere following the methodology described in [35]. In this study, $a_{cdm}(443)$ was only used for water-type classification purposes.

There are 148 data records containing contemporaneous observations of Chl and $R_{rs}(\lambda)$ from these five cruises, and the number of coincident $a_{cdm}(443)$ is 96.

Data collected through PPARR (Primary Production Algorithm Round-Robin) in this study was used for comparison purposes with the satellite climatology products only. In short, at each station, surface Chl was measured via the fluorometric method between 0 and 5 m depth, while PP was measured at various depths using ^{13}C- or ^{14}C-labeled compounds. Details were described at [36]. The numbers of stations, sampling dates, sampling regions and data sources for all expeditions are summarized in Table 1 while the locations of sampling stations are shown in Figure 1.

Table 1. Summary of in *situ* datasets.

Data	Station	Year	Month	Region	Source
MALINA	37	2009	July-August	Southern Beaufort Sea	SeaBASS
ICESCAPE2010	34	2010	June-July	Chukchi and Beaufort Sea	SeaBASS
ICESCAPE2011	16	2011	June-July	Chukchi and Beaufort Sea	SeaBASS
TARA	27	2013	May-November	Polar circle	SeaBASS
GREEN EDGE	34	2016	June-July	Baffin Bay	Individual
PPARR	973	1959-2011	August	Arctic Ocean	NOAA NCEI

Preprints (www.preprints.org) | NOT PEER-REVIEWED | Posted: 25 December 2023 doi:10.20944/preprints202312.1775.v1

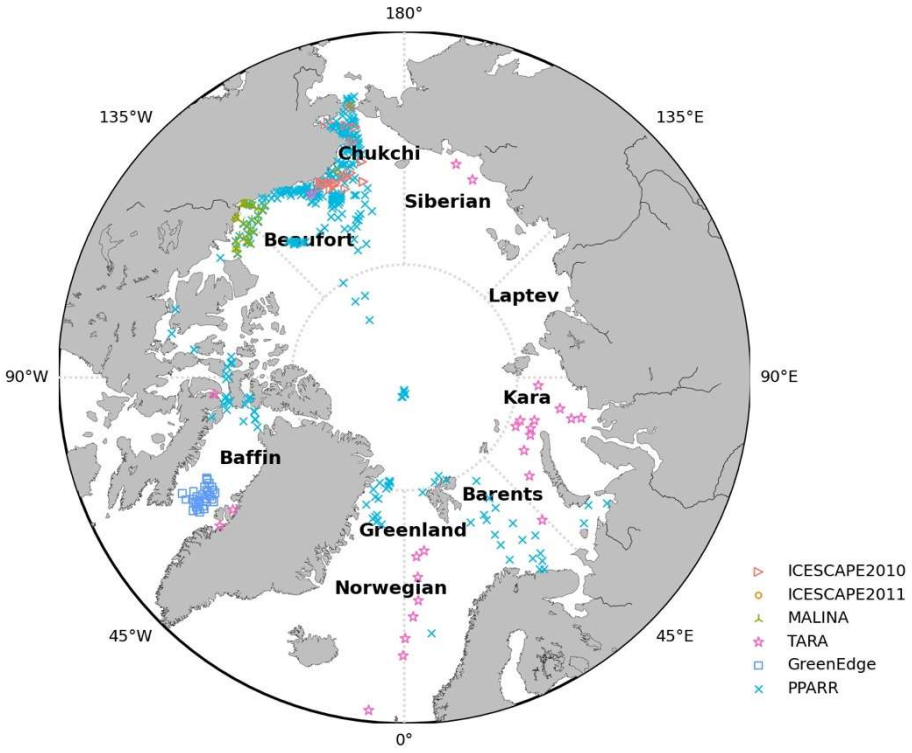

Figure 1. Map of the Arctic Ocean showing the locations of stations from various datasets.

To evaluate algorithms from the perspective of the impact of CDM, we arbitrarily split the algorithm-evaluation dataset into 4 water types. For this purpose, missing a_{cdm} (443) was estimated according to [37]. Then based on the measured median value of Chl (0.35 mg m^{-3}), we split the *in situ* dataset in half. For the half with Chl $\leq$ 0.35 mg m^{-3}, samples with $a_{cdm}(443) \leq 0.067$ m^{-1} were classified as chl.acdm while those with $a_{cdm}(443) > 0.067$ m^{-1} were regarded as chl.ACDM. The same procedure was applied to the other half of the dataset with Chl > 0.35 mg m^{-3}, thus deriving CHL.acdm and CHL.ACDM. This classification approach is illustrated in Figure 2 and Table 2.

Table 2. Classification criteria.

Water type	Threshold	Number
chl.acdm	Chl ≤ 0.35 mg m^{-3}, $a_{cdm}(443) \leq 0.067$ m^{-1}	48
CHL.acdm	Chl > 0.35 mg m^{-3}, $a_{cdm}(443) \leq 0.067$ m^{-1}	26
chl.ACDM	Chl ≤ 0.35 mg m^{-3}, $a_{cdm}(443) > 0.067$ m^{-1}	26
CHL.ACDM	Chl > 0.35 mg m^{-3}, $a_{cdm}(443) > 0.067$ m^{-1}	48

Preprints (www.preprints.org) | NOT PEER-REVIEWED | Posted: 25 December 2023 doi:10.20944/preprints202312.1775.v1

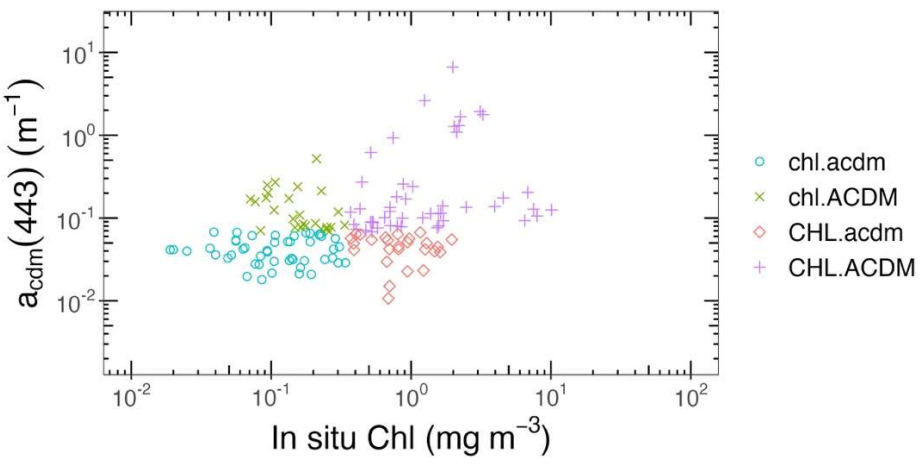

Figure 2. This scatter plot illustrates water-type classification according to the level of $a_{cdm}(443)$ and Chl in the water column.

2.2. Satellite products

OC-CCI (Ocean Color Climate Change Initiative, https://esa-oceancolour-cci.org/) L3b daily chlorophyll ***a*** products and reflectance products, and MODIS atmospheric products (MYD08, https://ladsweb.modaps.eosdis.nasa.gov) in August from 2003 to 2018, were downloaded to generate climatology Chl and PP products for the AO. Note that the OC-CCI chlorophyll ***a*** products are merged products based on SeaWiFS (Sea-viewing Wide Field-of-view Sensor), MERIS (Medium Resolution Imaging Spectrometer), aqua-MODIS (Moderate Resolution Imaging Spectroradiometer) and VIIRS (Visible Infrared Imaging Radiometer Suite) data to obtain as many pixels as possible, and Chl values are calculated by blending algorithms based on the water types as documented in ATBD-OCAB (Algorithm Theoretical Baseline Document-Ocean Color Algorithm Blending, [38]), which is substantially an empirical approach.

3. Methods

3.1. Descriptions of existing operational ocean-color algorithms

In this study, global empirical algorithms for SeaWiFS (OC4v6), MODIS (OC3Mv6) and VIIRS (OC3V), two regional empirical algorithms (OC4L and OC4P), one AO empirical algorithm (AO.emp), and two semi-analytical algorithms (GSM01 and GSM.AO) were evaluated.

3.1.1. Empirical algorithms

All empirical algorithms use polynomial functions to fit the relationship between Chl and the maximum blue-to-green ratio of remote-sensing reflectance:

$$Chl = 10^{a_0+a_1R+a_2R^2+a_3R^3+a_4R^4}, (1)$$

where R is the base 10 logarithm of the maximum blue-to-green band ratio of R_{rs} and a_i is an empirically-derived coefficient from the list in Table 3.

Table 3. Band configurations and coefficients of the empirical chlorophyll *a* algorithms evaluated.

Preprints (www.preprints.org) | NOT PEER-REVIEWED | Posted: 25 December 2023 doi:10.20944/preprints202312.1775.v1

Algorithms	Blue	Green	a_0	a_1	a_2	a_3	a_4
OC3Mv6	443>488	547	0.2424	-2.7423	1.8017	0.0015	-1.2280
OC3V	443>486	551	0.2228	-2.4683	1.5867	-0.4275	-0.7768
OC4v6	443>490>510	555	0.3272	-2.9940	2.7218	-1.2259	-0.5683
OC4P	443>490>510	555	0.2710	-6.2780	26.29	-60.94	45.31
OC4L	443>490>510	555	0.5920	-3.6070	-	-	-
AO.emp	443>490>510	555	0.1746	-2.8293	0.6592	-	-

Note that the wavelengths used for the blue and green bands vary slightly among sensors (see Table 3) and were designed for different water bodies. OC3Mv6, OC4v6, and OC3V were obtained using a global *in situ* dataset mainly from Case 1 and non-polar waters [21,22]. OC4P and OC4L were tuned using *in situ* measurements made in Canadian Arctic waters (in the vicinity of Resolute Bay and in the Labrador Sea, [23]), and the Western Arctic (Chukchi and Beaufort Seas, [19]), respectively. AO.emp was optimized using a large dataset compiled at a pan-Arctic scale [18,39].

3.1.2. Semi-analytical algorithm – GSM

The GSM semi-analytical ocean-color model was initially developed by [40] and later updated by [24] for SeaWiFS over non-polar Case 1 waters. The basic principle is to minimize the difference between the measured and modeled below-surface remote-sensing reflectance r_{rs} using non-linear optimization until a predefined convergence threshold is met. A detailed description of the GSM01 model and values of model parameters can be found in [24].

The GSM model can be tuned easily by reparameterizing model parameters using bio-optical data. [18] optimized the model parameters using a genetic optimization method for the AO based on the Arctic dataset described in [39], and the tuned model was named AO.GSM. Lewis et al. thus found that the optimized parameters more accurately represent the AO's unique bio-optical characteristics. Details of the genetic optimization procedure and parameter values were described in [18].

3.2 Evaluation criteria

The performance of each ocean-color algorithm was assessed following the metrics described in [41]. The first of these is the number of effective retrievals, n. For example, GSM01 may generate negative Chl values due to the optimization regime, these negative retrievals were considered as failures. The next two metrics are bias and mean absolute error (MAE), which have been proven to be robust and straightforward metrics for evaluating ocean-color algorithms with non-Gaussian distributions and outliers [41]:

$$bias = 10^{mean\left(log10(X^M)-log10(X^E)\right)}, and (2)$$

$$MAE = 10^{mean|log10(X^M)-log\quad(X^E)|}. (3)$$

Bias illustrates the systematic direction of error, as either underestimation or overestimation on average. A bias close to 1 means minimum bias, while a value lower than 1 reflects underestimation. A bias of 0.8 for instance reflects an average of 20% underestimation. The same reasoning holds for overestimations. MAE indicates random error and is always larger than 1. For instance, a MAE of 1.2 means average 20% relative error in retrievals compared to measured values.

The fourth metric is wins, which is obtained through pairwise comparison. That is, for each pair of estimated and measured variables, residuals (defined as estimated value minus measured value) for model A and model B are calculated, and the model with the lower residual is the winner while models that fail are directly designated as losers. Wins, described as the percentage of winners to the

Preprints (www.preprints.org) | NOT PEER-REVIEWED | Posted: 25 December 2023 doi:10.20944/preprints202312.1775.v1

total number of pairs, can be used to tell which model performs better and help to decide which model should be used in applications.

In addition, the slope and coefficient of determination (r^2) for log-transformed variables were also produced via type II reduced major axis (RMA) regression [42] as complementary metrics.

3.3. Primary-production model

The spectrally-resolved primary-production model for the Arctic waters developed by [16] was adopted in the present study. One advantage of this model compared to others [15,43,44] is its consideration of the propagation of spectral light in the atmosphere and the ocean using methods appropriate for both Case 1 and Case 2 waters. In recent years, this model has been further optimized to account for subsurface chlorophyll a maxima often observed in the AO. This was achieved by using the statistical relationships between Chl at surface and at depth, published by [45]. Furthermore, instead of using R_{rs} and Chl data from the GlobColour dataset as in [16], the present study used $R_{rs}(\lambda)$ merged products based on SeaWiFS, MERIS, aqua-MODIS and VIIRS data from OC-CCI for better coverage, and derived Chl products through the merged $R_{rs}(\lambda)$ products using the above-mentioned chlorophyll a algorithms.

The structure of this spectrally- and vertically-resolved Arctic primary-production model is illustrated in Figure 3. Basically, the daily rates of PP carbon fixation by phytoplankton cells in units of mgC m^{-2} d^{-1} are estimated using the classic photosynthesis versus light model [46]:

$$PP = P_B^{max} \int_{t=0}^{24h} \int_{z_{0.1\%}}^{z_{100\%}} Chl(z) \left(1 - e^{-\frac{PUR(z,t)}{E_k(PUR)}}\right) dz dt, \qquad (4)$$

where P_B^{max} (mgC mgChl^{-1} h^{-1}) is the light-saturated chlorophyll-normalized carbon-fixation rate, which is assumed as being constant at 2.0 mgC mgChl^{-1} h^{-1} (see [16] and references therein). Chl(z) is chlorophyll a concentration at a given depth z, which can be propagated from surface values following [45]. $PUR(z,t)$ is photosynthetically usable radiation expressed in µmol photons m^{-2} s^{-1} [47], which can be estimated using input atmospheric data and satellite-observed $R_{rs}(\lambda)$, and the spectral model of light propagation through the atmosphere and ocean has been described in [16]. $E_k(z)$ (µmol photons m^{-2} s^{-1}) is the saturation irradiance, parameterized here as a function of PUR(z,t) [16].

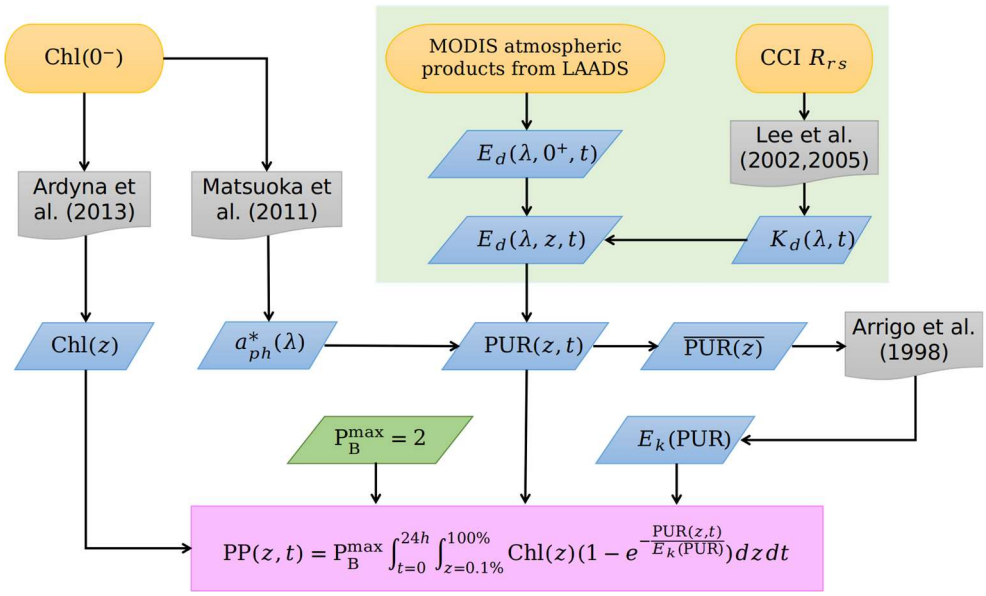

Figure 3. Structure of the spectrally- and vertically-resolved Arctic primary-production model. Yellow, gray, blue, green and magenta frames refer to model inputs, methods described in literature, intermediate variables, constant values and photosynthesis model, respectively (courtesy of Marcel Babin and Simon Bélanger).

 doi:10.20944/preprints202312.1775.v1

To quantify the impact of Chl retrievals derived from various algorithms on PP estimates, we performed a sensitivity analysis using an Arctic primary-production model as described below. In short, measured Chl and $R_{rs}(\lambda)$ along with temporally- and geographically-matched atmospheric parameters were inputted into the Arctic primary-production model to derive spectrally- and vertically-resolved PP (named as PP-Ref). Subsequently, the Chl input alone was replaced by the Chl estimates derived through the various above-mentioned chlorophyll *a* algorithms, using measured $R_{rs}(\lambda)$ to obtain PP estimates (named as PP-Algorithm; for instance, PP generated via OC4L-derived Chl was referred to as PP-OC4L). Note that since the primary-product model is a bin-based approach, several samples might be projected to the same bin; therefore, the total number of PP estimates is 135 rather than 148. Also note that in this model, PP is not exactly proportional to Chl (Figure 3).

3.4. Climatology products

The Chl climatology product in August was obtained by averaging all the OC-CCI daily Chl products collected in August from 2003 to 2018. Meanwhile, to obtain the PP climatology product in August, firstly, each daily Chl product acquired in August was entered into the Arctic primary-production model (described in Section 2.4) along with the corresponding daily reflectance product and MODIS atmospheric product to derive the daily PP product; then, all the daily PP products were averaged to calculate the climatology PP product.

3.5. Matchup analysis

The algorithm-evaluation dataset was firstly matched with PPARR to search for concurrent measurements of both Chl and PP. This *in situ* dataset was then compared with daily Chl and PP products (described in Section 3.4) to look for temporal- and spatial-matched pairs. Concretely, this meant, for each *in situ* entry, keeping only the closest (within 4km) satellite data obtained on the same day. Finally, only 5 *in situ* and satellite matchups were thus identified due to the lack of *in situ* measurements in the AO.

4. Results

4.1. Overview of product performance

Given the lack of *in situ* and satellite matchups, the accuracy of Chl products at a pan-Arctic scale was generally assessed by comparing the climatology Chl product in August (Figure 4a) with the *in situ* Chl measurements taken in August from PPARR via a kernel density plot (Figure 4b). It was found that the Chl product tends to generate higher estimates (median Chl=0.66 mg m^{-3}) compared with the *in situ* values (median Chl=0.40 mg m^{-3}), especially in the section where Chl<1.2 mg m^{-3} (accounting for nearly 2/3 of all pixels). This comparison also yielded a small percentage of visibly higher estimates in the 4.0 to 11.0 mg m^{-3} range. By referring to the Chl distribution shown in Figure 4a, we can see that this proportion of higher estimates can be attributed to areas in and around the large river plumes which hold considerabl amounts of CDM as a result of river discharge.

Preprints (www.preprints.org) | NOT PEER-REVIEWED | Posted: 25 December 2023 doi:10.20944/preprints202312.1775.v1

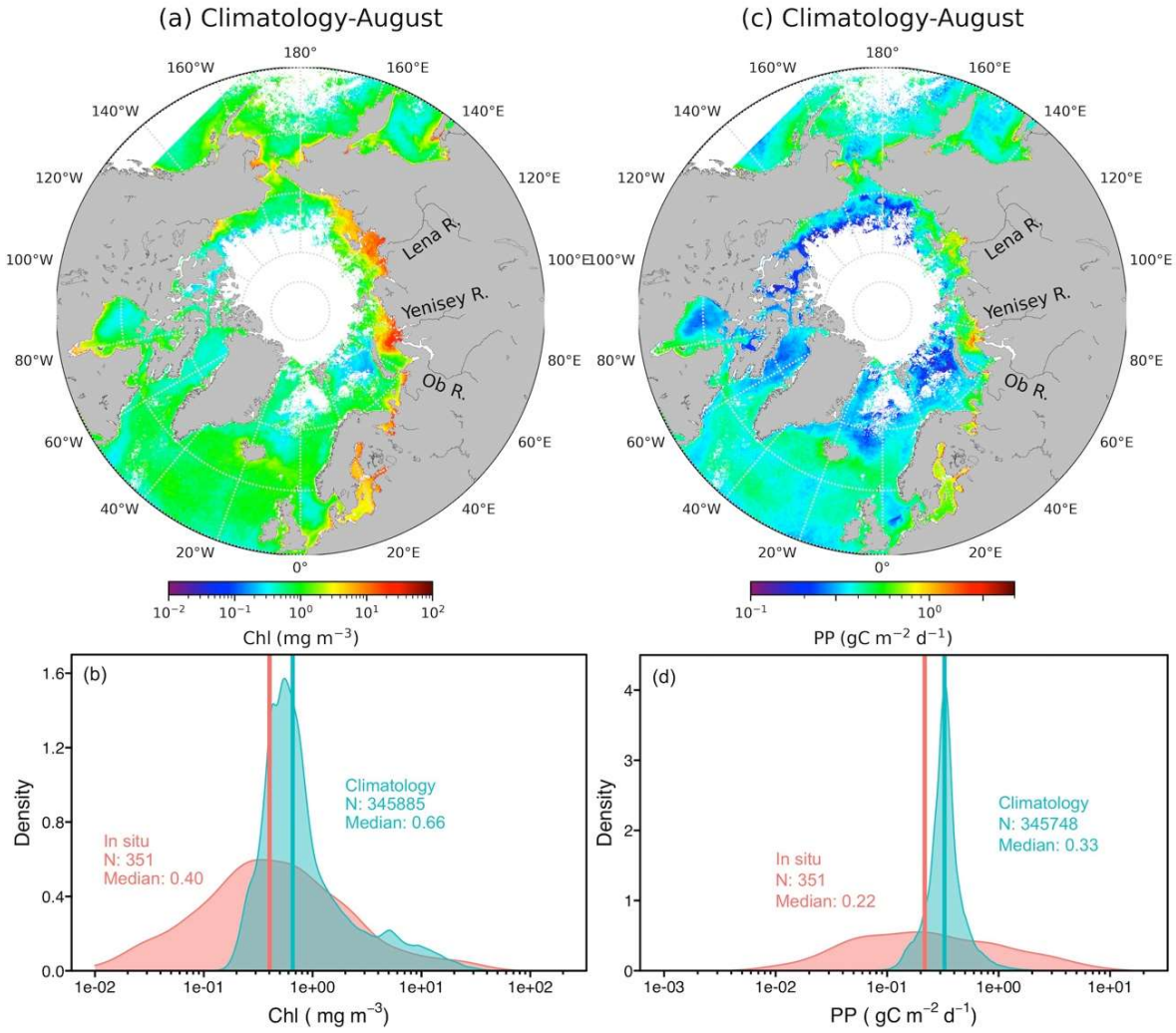

Figure 4. (**a**) Climatology chlorophyll product in August derived through the blended empirical algorithm; (**b**) kernel density plot of Chl measurements collected in August from PPARR (red) and Chl climatology product in August (green); (**c**) climatology primary product in August produced through the Arctic primary-production model using OC-CCI daily reflectance and chlorophyll products; (**d**) kernel density plot of PP measurements collected in August from PPARR (red) and PP climatology product in August (green).

The corresponding climatology PP product is shown in Figure 4c, and the density curve compared with PP measurements from PPARR (same pairs of Chl measurements shown in Figure 4b) is illustrated in Figure 4d. As in the case of Chl estimates, PP estimates were also higher overall (median PP=0.33 gC $m^{-2}d^{-1}$) in comparison with *in situ* values (median PP=0.22 gC $m^{-2}d^{-1}$). Only one crest was recorded, located at 0.33 gC $m^{-2}d^{-1}$. One-third of all the PP estimates in the 0.007 to 0.2 gC $m^{-2}d^{-1}$ range were higher than the measurements, which is likely due to the higher Chl estimates. In the higher range (PP>0.6 gC $m^{-2}d^{-1}$) however, another one-third of PP estimates were lower than measurements. The higher estimates on the left side and lower estimates on the right side steepened the crest, resulting in the density at the crest as being nearly 8 times that of the *in situ* one. Significantly, the higher Chl estimates in and around large river plumes did not lead to higher PP estimates. It is likely that the high proportion of CDM in the water column was extremely absorbent of sunlight, thereby resulting in less PUR for absorption by phytoplankton [48].

4.2. Bio-optical algorithm evaluations

Preprints (www.preprints.org) | NOT PEER-REVIEWED | Posted: 25 December 2023 doi:10.20944/preprints202312.1775.v1

Chl is one of the key variables influencing PP estimates [16]. Since several chlorophyll a algorithms are available, their relative performance needs to be examined first. Figure 5 shows the comparison between measured and estimated Chl using the various algorithms mentioned above for the 4 water types (see definition in Section 2.3). Overall, all the algorithms showed a trend of overestimation. OC4v6 and OC4L boosted estimations the most, overestimating by 132% whereas OC4P was the least biased but had the largest MAE (Table 4). The MAE of AO.GSM was the smallest, followed by GSM01 and AO.emp, and lastly by the three global algorithms. The MAE of OC4L was noticeably larger than that of the global algorithms, indicating that the regional Arctic empirical algorithm was not suitable for the pan-Arctic Ocean as regional algorithms are subject to the compatibility of the waters under study with the waters from which data were obtained for algorithm development. As for the performance of regression, AO.GSM had the largest r^2, but its slope was not as close to 1 as that of the other algorithms except for the two Arctic regional algorithms OC4P and OC4L.

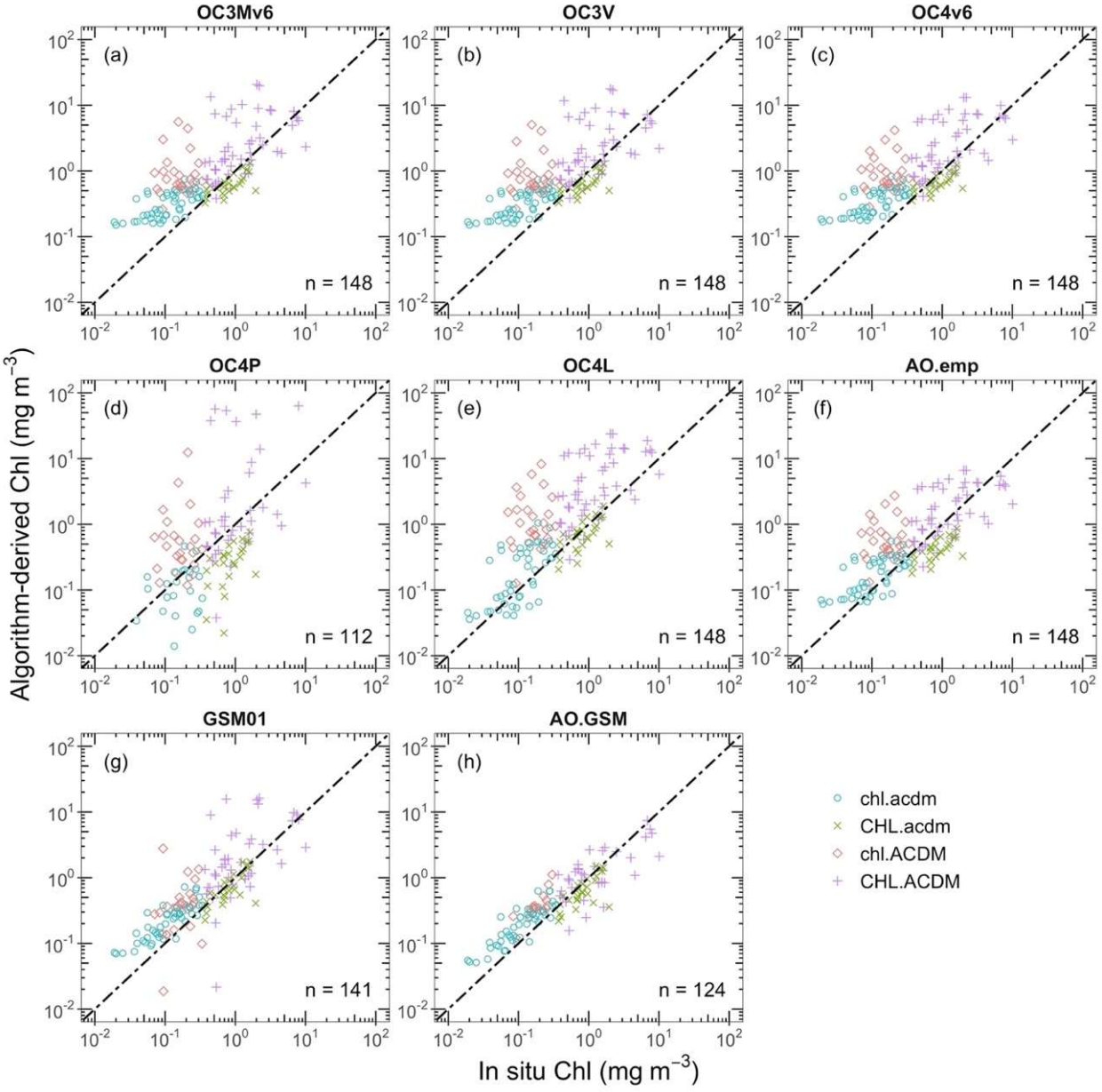

Figure 5. Comparisons between measured and estimated Chl for individual chlorophyll *a* algorithms at 4 water types (see Table 2 for definition).

Table 4. Performance metrics of the various algorithms evaluated.

Preprints (www.preprints.org) | NOT PEER-REVIEWED | Posted: 25 December 2023 doi:10.20944/preprints202312.1775.v1

Algorithm	n	bias	MAE	Overall Wins (%)	r^2	slope
OC3Mv6	148	2.22	2.68	48.9	0.49	0.86
OC3V	148	2.17	2.64	48.0	0.49	0.83
OC4v6	148	2.32	2.75	37.2	0.52	0.83
OC4P	112	1.08	3.16	38.8	0.21	1.61
OC4L	148	2.30	2.82	43.2	0.55	1.28
AO.emp	148	1.36	2.15	65.6	0.54	0.92
GSM01	141	1.59	2.08	58.6	0.62	0.97
AO.GSM	124	1.24	1.73	58.0	0.79	0.77

To rank the overall performances of all the algorithms tested, percent wins between every pair combination of two algorithms were calculated (Table 5). Among the three global algorithms, OC3Mv6 performed the best and OC4v6 the worst. They all outperformed the two regional Arctic algorithms, but lost when compared with AO.emp, GSM01 and AO.GSM. OC4L only performed better than OC4P which had the worst overall performance. As for GSM01, it outperformed the other algorithms except for AO.emp and AO.GSM. The percent wins of AO.emp were equal to those of AO.GSM. However, AO.emp emerged with a larger proportion of overall wins (65.6%). In this way, AO.emp was the best algorithm among all tested in the present study.

Table 5. Algorithm performance assessed through pair-to-pair comparison.

	Percent Wins							
Algorithm	**OC3Mv6**	**OC3V**	**OC4v6**	**OC4P**	**OC4L**	**AO.emp**	**GSM01**	**AO.GSM**
OC3Mv6	-	46.6	27.7	39.9	41.9	72.3	66.9	62.2
OC3V	53.4	-	29.1	39.2	42.6	71.6	67.6	60.8
OC4v6	72.3	70.9	-	39.2	46.6	73.0	73.0	64.9
OC4P	60.1	60.8	60.8	-	56.1	67.6	60.8	55.4
OC4L	58.1	57.4	53.4	43.9	-	67.6	63.5	53.4
AO.emp	27.7	28.4	27.0	32.4	32.4	-	42.6	50.0
GSM01	33.1	32.4	27.0	37.2	36.5	57.4	-	59.5
AO.GSM	37.8	39.2	35.1	39.9	46.6	50.0	35.8	-
Overall Wins	48.9	48.0	37.2	38.8	43.2	65.6	58.6	58.0
Failure				36 (24.3%)			7 (4.7%)	24 (16.2%)

When taking a closer look at the different water types, symbols representing waters with high CDM (i.e. 'diamonds' for chl.ACDM and 'pluses' for CHL.ACDM) are distributed in a more scattered fashion than those for waters with low CDM for all empirical algorithms and GSM01 (Figure 5). However, this phenomenon is not visible for AO.GSM, namely because for waters with high CDM, this algorithm obtained 24 failures (accounting for 16.2% of the total sample), which were thus

Preprints (www.preprints.org) | NOT PEER-REVIEWED | Posted: 25 December 2023 doi:10.20944/preprints202312.1775.v1

excluded from the comparisons (see Figure 7 and Table 6). In other words, AO.GSM is more likely to fail for waters with high CDM. These findings indicate that a high proportion of CDM in the water column is the main obstacle to success for these empirical and semi-analytical algorithms.

Table 6. Performance metrics of GSM01 and AO.GSM by individual water type and across all water types.

Water Type	Algorithm	n	bias	MAE	Wins (%)	Failure	r^2	slope
chl.acdm	GSM01	48	1.96	1.99	6.2		0.71	0.85
	AO.GSM	48	1.74	1.78	93.8		0.75	0.92
CHL.acdm	GSM01	26	0.83	1.33	69.2		0.52	1.09
	AO.GSM	26	0.74	1.41	30.8		0.50	1.11
chl.ACDM	GSM01	24	2.10	2.72	34.6	2 (7.7%)	0.08	1.03
	AO.GSM	15	2.02	2.02	57.7	11 (42.3%)	0.65	1.25
CHL.ACDM	GSM01	43	1.57	2.45	47.9	5 (10.4%)	0.27	1.03
	AO.GSM	35	0.92	1.81	41.7	13 (27.1%)	0.47	0.79
Across all	GSM01 *	124	1.47	1.81	29.0		0.80	0.81
	AO.GSM	124	1.24	1.73	71.0		0.79	0.77

* Subset of GSM01-derived retrievals with data common to that of AO.GSM.

Boxplots were deployed to quantify the difference between measured and estimated Chl by individual algorithms for each water type (Figure 6). The MAEs were also labeled. Generally, the MAE of most of the algorithms tested (except OC4P and AO.emp) was the smallest for CHL.acdm (1.33 to 1.44), but the largest for chl.ACDM (2.02 to 7.11). Combined with the finding that the MAE for chl.acdm was smaller than that for CHL.ACDM, our results suggest that the higher the level of CDM in relation to Chl, the greater the uncertainties surrounding Chl estimates. Given that OC4P had the largest MAE (3.16) and the most failures (24.3%), it is hereafter excluded from further analysis.

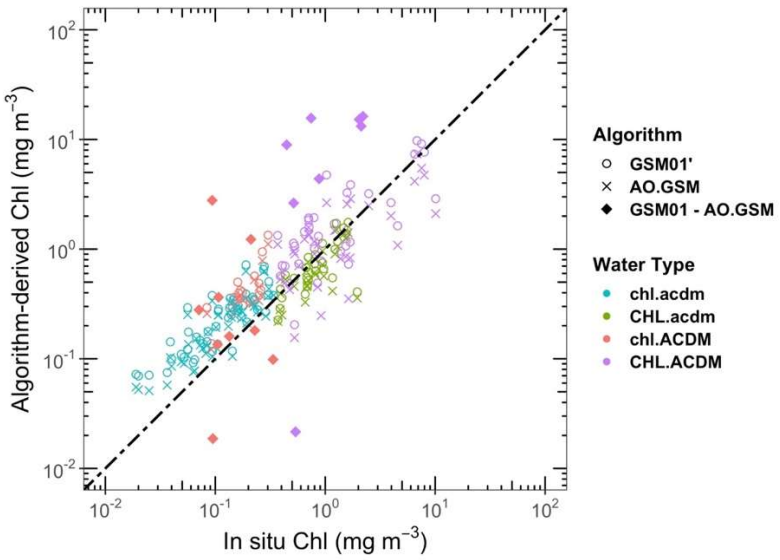

Preprints (www.preprints.org) | NOT PEER-REVIEWED | Posted: 25 December 2023 doi:10.20944/preprints202312.1775.v1

Figure 6. Pair-to-pair comparison between GSM01 and AO.GSM, circles and x symbols refer to the same data pairs derived from GSM01 and AO.GSM, diamonds refer to the data failed using AO.GSM but succeeding using GSM01.

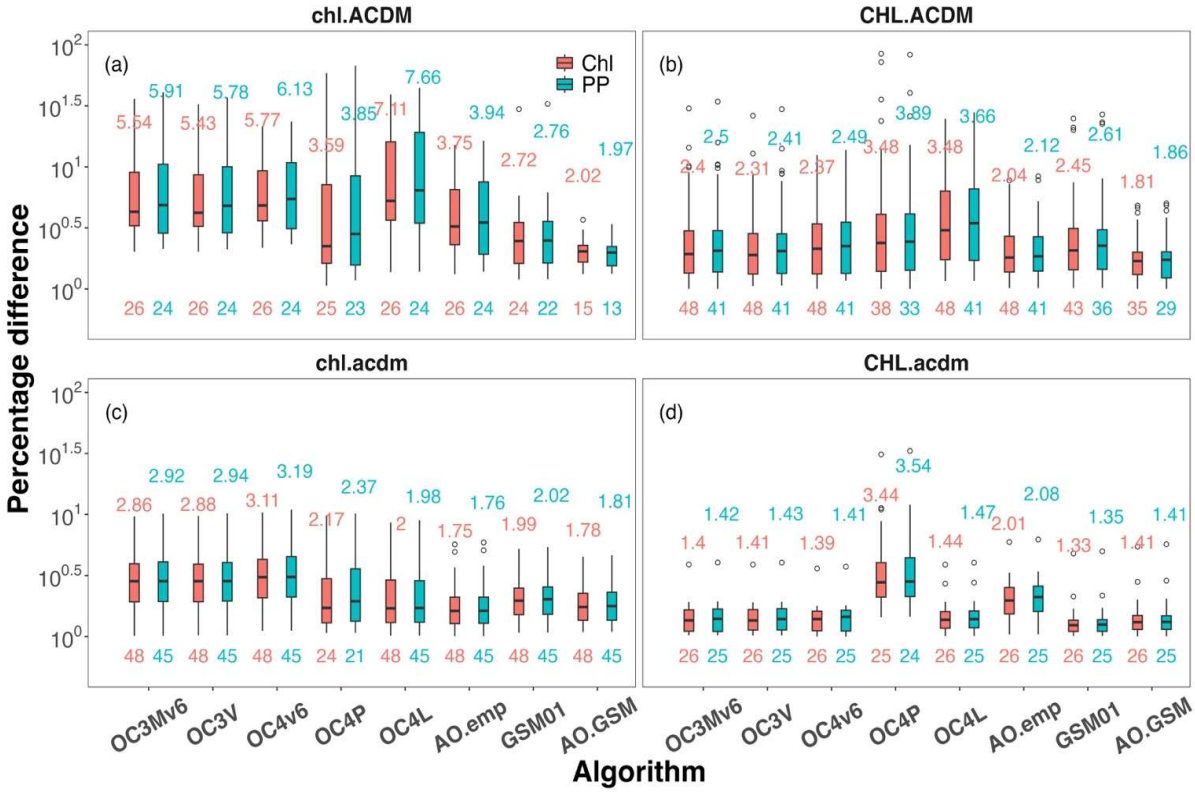

Figure 7. Boxplots of percentage difference between measured and estimated Chl (red), between PP derived using measured Chl and PP estimated from algorithm-derived Chl (green) for 4 water types (see Table 2 for definition). The labels above boxplots show MAE, those below show the numbers of samples classified as a certain water type.

For waters with low CDM (waters where $a_{cdm}(443) < 0.067$ m^{-1} in this study), the three global algorithms had the highest MAE, with values up to 2.86, followed by OC4L, GSM01 and AO.GSM for chl.acdm (Figure 6). AO.emp obtained the lowest MAE (1.75), but the largest MAE (2.01) for CHL.acdm, as confirmed by the notable underestimation shown by the 'x' symbols in Figure 5. The MAEs of the other algorithms were around only 1.4 for CHL.acdm, with GSM01 producing the smallest (1.33).

For waters with high CDM (i.e. chl.ACDM and CHL.ACDM), OC4L obtained the largest MAEs (7.11 and 3.48, respectively), indicating that this regional Arctic empirical algorithm is less applicable for CDM-rich waters than the global empirical algorithms. AO.emp yielded the smallest MAE among all empirical algorithms tested for waters with high CDM, but the contrary was found for CHL.acdm. It seems that empirical algorithms only consider the main characteristics of water bodies, and thus cannot work well for all types of waters. However, the two GSM models had the smallest MAEs for chl.ACDM, and obtained relatively good performances for other water types. It is therefore recommended that semi-analytical algorithms, such as GSM-like models, be used for CDM-rich waters even if they may produce failures.

To give a comprehensive comparison of the two GSM models, Table 6 summarizes their performance metrics for each water type. According to the wins, AO.GSM outperformed GSM01 for chl.acdm and chl.ACDM, but lost for CHL.acdm and CHL.ACDM. Figure 7 shows the pair-to-pair comparisons, with the diamond symbols representing the samples which failed with AO.GSM but succeeded with GSM01. The latter all belonged to water types with high CDM, and most of them were located far from the 1:1 regression line. When excluding these diamonds, AO.GSM

Preprints (www.preprints.org) | NOT PEER-REVIEWED | Posted: 25 December 2023 doi:10.20944/preprints202312.1775.v1

outperformed GSM01 with 71.0% wins (see Table 6). It was thus shown that AO.GSM has the ability to eliminate retrievals with poor performance.

In terms of overall wins, AO.emp was the best chlorophyll *a* algorithm tested. However, for waters with high CDM, which are of particular interest here, GSM-like models demonstrate better performance for the AO than empirical algorithms.

4.3. Impacts on PP estimates

Figure 8 shows the comparisons between PP-Ref and each PP-Algorithm (see Section 3.3 for definition). Generally, the comparisons of PP estimates followed the same trends as those for Chl. In other words, when Chl was overestimated, the corresponding PP-Algorithm also showed a trend of overestimation compared with PP-Ref. The same was also true for underestimation. It should be noted that the boundaries between water types grew blurry with respect to Chl level. For instance, some 'plus' symbols (see the black circle in Figure 8) representing water type CHL.ACDM were located to the left of some 'circle' and 'diamond' symbols which referred to waters with low Chl, indicating that PP for waters with low surface Chl can exceed that of waters with high surface Chl due to the possible existence of a prominent subsurface chlorophyll maximum.

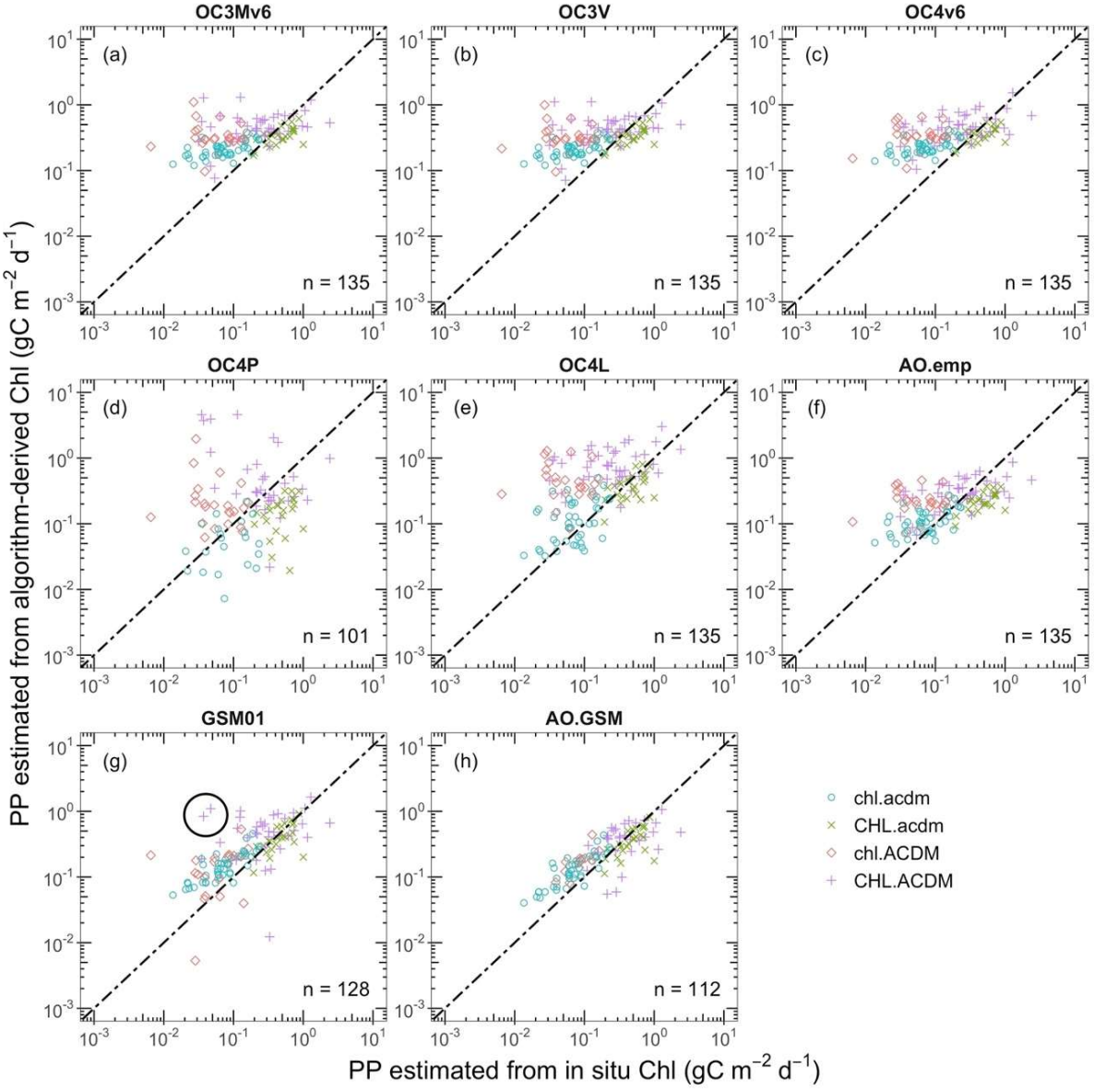

Preprints (www.preprints.org) | NOT PEER-REVIEWED | Posted: 25 December 2023 doi:10.20944/preprints202312.1775.v1

Figure 8. Comparisons between PP estimated from *in situ* Chl and PP estimated from algorithm-derived Chl for 4 water types (see Table 2 for definition). The black circle in Subfigure (g) is used to illustrate the mix of water types in terms of the level of Chl in the water column.

The same boxplots of percentage difference between PP-Ref and PP-Algorithm are shown in Figure 6. It can be seen that the percentage differences of PP followed the trend of Chl, and the rankings of MAE reflected those of Chl but with relative larger values. Taking the best algorithm AO.emp as an example, the MAEs of PP were 0.5%, 3.4%, 5.1%, and 3.9% larger than those of Chl for water types chl.acdm, CHL.acdm, chl.ACDM and CHL.ACDM, respectively. In addition, the amplifications of difference from Chl to PP were generally greater in waters with a relatively high proportion of CDM. Overall, considering all the algorithms, the amplification of difference from Chl to PP, largely due to the statistical approximation of the vertical Chl profile, did not exceed 7%.

In addition to the assessment of error propagation from Chl to PP, the impact of CDM on PP estimates was also explored through matchup analyses. Figure 9 shows the residual of PP estimates resulting from Chl errors for waters with different levels of CDM. For waters with comparable levels of Chl and CDM (i.e. water types chl.acdm and CHL.ACDM), PP absolute errors vary from 0.06 to 0.24 gC m^{-2} d^{-1}, which are lower values than for chl.ACDM. We can also note that a 399% overestimation of Chl (see the upper green symbol in Figure 9) merely led to 0.15 gC m^{-2} d^{-1} absolute error in PP for waters with low CDM whereas for waters with high CDM, a lower overestimation (199%) of Chl could result in a higher absolute error (0.62 gC m^{-2} d^{-1}). Meanwhile, a 484% overestimation of Chl induced an absolute error that went up to 2.3 gC m^{-2} d^{-1} in PP. In this way, a high CDM level (relative to Chl) in the water column may not only cause a larger error in the inversion of Chl, but also lead to a larger absolute error in the estimation of PP. While the Arctic primary-production model used in this study generally showed a trend of underestimation, especially for the water type chl.ACDM, more matchup analyses are needed to validate the Arctic PP model and to quantify the errors.

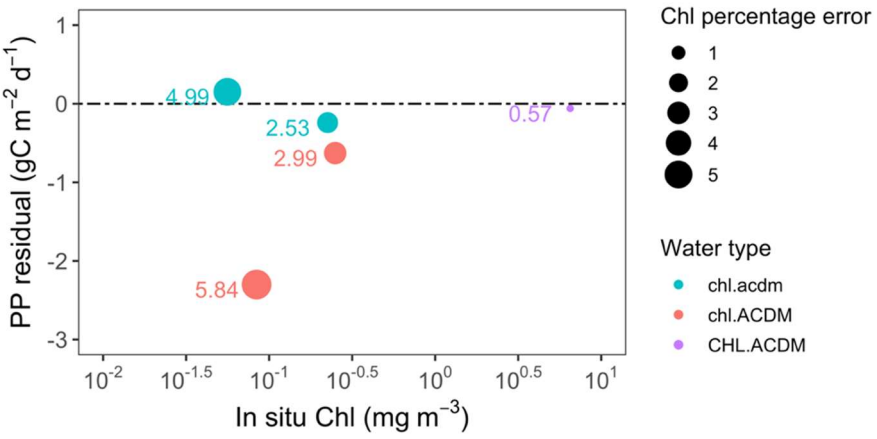

Figure 9. Relationship between PP absolute error (PP estimated from *in situ* Chl subtracted from measured PP) and *in situ* Chl through matchup analyses. Labels refer to percentage errors of Chl estimates. A value of 4.99 means overestimation by 399%, while a value of 0.57 reflects 43% underestimation.

5. Discussions and perspectives

5.1. Chl retrieval error

As far as the three global chlorophyll a algorithms, OC3Mv6, OC3V and OC4v6, are concerned, the assumed relationship between R_{rs} and Chl is problematic for the AO because the absorption properties of the latter are fundamentally different from those of typical Case 1 waters. Many studies [6–8,37,49–51] have documented that the non-water absorption of the AO is dominated by CDOM even at the phytoplankton absorption peak at 443 nm. In this way, the presence of CDOM at levels

 doi:10.20944/preprints202312.1775.v1

higher than the global mean will reduce the R_{rs} signal at blue wavelengths due to its strong absorption. As a consequence, global empirical algorithms using maximum blue-to-green R_{rs} ratios tend to have lower maximum band ratios, leading to an overestimation of Chl. Generally, the predominant influence of CDOM is to increase the intercept of the *in situ* versus algorithm-derived Chl regression and to only minimally change the slope [52].

In addition, as a consequence of the Arctic's photo-acclimation of low irradiance and cold temperatures, an increase in phytoplankton cell size and/or in intra-cellular pigment concentration decreases the light-absorption coefficient per unit Chl [6,8,19]. This higher package effect flattens the absorption spectrum of chlorophyll a, especially at the blue absorption peak. Thus, in contrast to the effect of CDOM, a relatively larger decrease in a_{ph}^{*} at blue wavelengths than at green wavelengths yields a larger maximum band ratio, leading to an underestimation of Chl when using global empirical algorithms for the AO. As a result, a relatively higher pigment-package effect decreases the slope of the *in situ* versus estimated Chl regression without significantly changing the intercept [52].

Overall, the difference between simulated and measured Chl is a consequence of the combined effects of Chl overestimation due to relatively higher CDOM absorption, and underestimation due to relatively higher pigment-package effects. In this study, the three global algorithms showed an obvious overestimation at all Chl ranges (Figure 5a-c), indicating that relatively higher CDOM absorption was the dominant factor that biased Chl estimates in the AO.

The failure of the two regional Arctic chlorophyll a algorithms was imputed to the significant spatial variance of bio-optical properties at a pan-Arctic scale. The AO is a spatially heterogeneous sea. In other words, the composition of non-water constituents and bio-optical properties significantly differs from region to region due to varying degrees of river inputs, nutrient levels, sea-ice coverage, shelf widths, and circulation patterns [37,52]. Hence, a single regional empirical algorithm, like OC4L or OC4P tuned for the Beaufort and Chukchi Seas, is not appropriate for the entire AO. This is likely reflected by the worse performances that these algorithms recorded compared to the global empirical algorithms evaluated in the present study (see Figure 5 and Table 4). Such a degree of variability makes it difficult to establish a standard empirical formulation that may provide robust predictions with acceptable error limits, at least on the scale of the entire Arctic region. This was the case of AO.emp. Although the MAE of AO.emp was lower than those of the other algorithms for chl.acdm, for CHL.acdm its MAE was even larger than those of the global algorithms. Thus, in theory, it is recommended to use a semi-analytical algorithm which compensates for optical properties in a given location through an optimization process and allows for discrimination and quantification of the roles of non-phytoplankton constituents in the optical properties of seawater, to improve the accuracy of Chl estimates from OCRS in polar waters.

The standard semi-analytical algorithm GSM01, with parameters optimized for non-polar Case 1 waters, could not properly represent the combination of water constituents in the AO. In other words, due to the high CDM proportion in the AO, the spectral slope for a_{cdm} should be sharper, and $a_{ph}^{*}(\lambda)$ should be lower to account for a higher package effect. This may be the reason why GSM01 performed worse than AO.emp (see Table 4). After reparameterizing for the AO, AO.GSM outperformed GSM01 in the pair-wise comparison and showed the lowest MAEs for water types chl.ACDM and CHL.ACDM. However, for these two water types, AO.GSM also had 24 failures, which represents 16.2% of the total samples. Future research should therefore aim for a chlorophyll a algorithm which can produce as many effective retrievals with reasonable uncertainty.

5.2. PP estimate error

PP was estimated in the present study using the classic photosynthesis versus light model based on the integration of carbon fixation by phytoplanktonic cells. The prime determinant of PP variations for ice-free waters in such models designed for OCRS data is Chl, except during seasons when incident irradiance becomes highly limiting. It is expected that errors in Chl should mostly propagate proportionally to PP, especially when all other variables are kept constant from one set of simulations to another, as in our study. In the model we used, however, Chl also drives the vertical distribution of chlorophyll concentration, as well as the chlorophyll-specific absorption coefficient of

Preprints (www.preprints.org) | NOT PEER-REVIEWED | Posted: 25 December 2023 doi:10.20944/preprints202312.1775.v1

phytoplankton. Nevertheless, our results suggest and largely confirm that errors in Chl mostly propagate proportionally to PP.

In the present study, since we only obtained 5 *in situ* and satellite-derived PP matchups, we further compared the PP estimates produced from the algorithm-evaluation dataset with the *in situ* PP from PPARR to assess their accuracy. Figure 10a shows the relationship between *in situ* PP and Chl using the PPARR dataset. It can be seen that, in the range from 0.1 to 1.0 mg m^{-3}, PP varied across three orders from 0.01 to 10.0 gC m^{-2} d^{-1}. In addition, for Chl<6.0 mg m^{-3}, the triangle symbols were likely to be evenly distributed along the regression line, while for Chl>6.0 mg m^{-3}, all triangles lay below the regression line. Figure 10b illustrates the relationship between estimated PP and measured Chl using the algorithm-evaluation dataset, duplicating the regression line of Figure 10a for the purpose of comparison. For waters with low CDM (i.e. water types chl.acdm and CHL.acdm), the estimated PP fitted the *in situ* regression line well. Meanwhile, for CDM-rich waters, PP estimates were more likely to be located at the bottom-right of the regression line, especially for CHL.ACDM which is located the farthest from the regression line. It seems that chlorophyll-specific PP in CDM-rich waters is relatively lower than in waters with low CDM. In addition, various vertical Chl profiles with the same surface value may lead to significant variance in the estimation of PP. Therefore, remote sensing of detectable Chl vertical structures is still expected to obtain more accurate PP estimates in the future, and more *in situ* and satellite matchups are needed to quantify their accuracy.

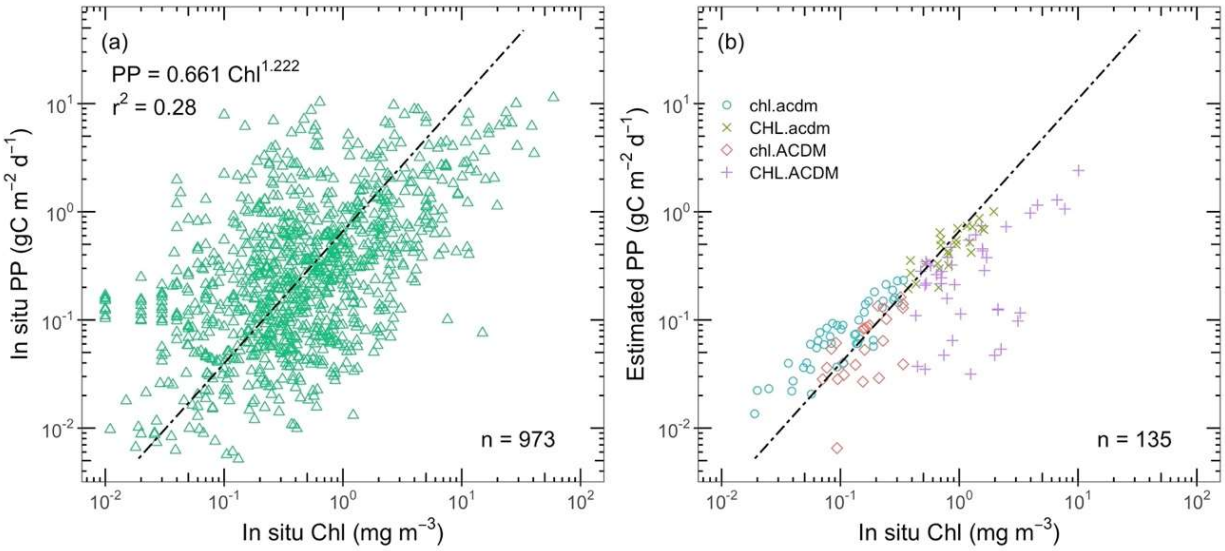

Figure 10. (**a**) Relationship between *in situ* PP and Chl from PPARR; (**b**) relationship between PP estimates and *in situ* Chl using the dataset used for algorithm evaluation. The black dashed line is the regression line between *in situ* PP and Chl from PPARR.

5.3. Conclusion

Given that the poor performance of standard empirical algorithms in the AO is due to the interference of CDM in phytoplankton signals in the visible spectrum, in this study we evaluated currently available algorithms to investigate the impact of CDM. We found that the higher the level of CDM in relation to Chl in the water column, the larger the bias in the estimation of Chl. Overall, AO.emp performed the best among all the algorithms tested, but for the CDM-rich waters of greatest interest here, GSM models performed better than all the empirical algorithms. Therefore, the use of an empirical algorithm for the entire AO should be avoided when possible. It is recommended that semi-analytical algorithms (such as GSM-like models) be used instead, as they can discriminate and quantify the roles of non-phytoplankton constituents for the heterogeneous AO. Nevertheless, given that AO.GSM is more likely to fail for waters with high CDM, future research is required to develop another semi-analytical algorithm that can produce as many possible effective retrievals with reasonable uncertainty.

Through analysis of the sensitivity of PP estimations to Chl, we found that errors in Chl mostly propagate proportionally to PP, and were slightly amplified (<7%) mainly due to the statistically vertically-resolved Chl profile. In addition, matchup analysis allowed us to find that PP absolute error was much larger for CDM-rich waters. For instance, a 399% overestimation of Chl for waters with low CDM merely led to 0.15 gC m^{-2} d^{-1} absolute error in PP, while for waters with high CDM, PP absolute error could reach up to 2.3 gC m^{-2} d^{-1} with an overestimation of Chl by 484%. It was also discovered that the spectrally- and vertically-resolved Arctic primary-production model used in this study underestimated PP to some extent. Overall, our PP calculations provide a quantitative indication of the uncertainty in PP estimates that can be expected in the Arctic, for different seawater optical categories as defined here.

Author Contributions: Conceptualization, Marcel Babin, Atsushi Matsuoka, Xiaoping Pang and Juan Li; methodology, Marcel Babin and Juan Li; software, Juan Li and Phillipe Massicotte; validation, Juan Li; formal analysis, Juan Li; investigation, Juan Li; resources, Marcel Babin and Atsushi Matsuoka; data curation, Marcel Babin, Atsushi Matsuoka and Juan Li; writing—original draft preparation, Juan Li; writing—review and editing, Marcel Babin, Atsushi Matsuoka, Xiaoping Pang, Phillipe Massicotte and Juan Li; visualization, Juan Li; supervision, Marcel Babin, Atsushi Matsuoka and Xiaoping Pang; project administration, Marcel Babin; funding acquisition, Marcel Babin, Atsushi Matsuoka and Xiaoping Pang. All authors have read and agreed to the published version of the manuscript.

Funding: This research was funded by the Sentinel North program of Université Laval (Canada First Research Excellence Fund), ArcticNet, SMAART, CNES (French space agency), and Marcel Babin's NSERC Discovery Grant. Parts of this research were supported by a NASA ROSES project (subcontract #1658689 of the prime contract awarded to Jet Propulsion Laboratory, California Institute of Technology, 80NM0018D0004 between Caltech and NASA) and the Japan Aerospace Exploration Agency (JAXA) Global Change Observation Mission-Climate contract awarded to Atsushi Matsuoka (GCOM-C; contract #22RT000298).

Data Availability Statement: The datasets used in this study can be found at MALINA [25], ICESCAPEs [26], TARA [27], GREEN EDGE [28], and PPARR [36].

Conflicts of Interest: The authors declare no conflict of interests.

References

1. Carmack, E.C.; Yamamoto-Kawai, M.; Haine, T.W.; Bacon, S.; Bluhm, B.A.; Lique, C.; Melling, H.; Polyakov, I.V.; Straneo, F.; Timmermans, M.-L.; et al. Freshwater and Its Role in the Arctic Marine System: Sources, Disposition, Storage, Export, and Physical and Biogeochemical Consequences in the Arctic and Global Oceans. *Journal of Geophysical Research: Biogeosciences* **2016**, *121*, 675–717, doi:10.1002/2015JG003140.
2. Peterson, B.J.; Holmes, R.M.; McClelland, J.W.; Vörösmarty, C.J.; Lammers, R.B.; Shiklomanov, A.I.; Shiklomanov, I.A.; Rahmstorf, S. Increasing River Discharge to the Arctic Ocean. *Science* **2002**, *298*, 2171–2173, doi:10.1126/science.1077445.
3. Raymond, P.A.; McClelland, J.W.; Holmes, R.M.; Zhulidov, A.V.; Mull, K.; Peterson, B.J.; Striegl, R.G.; Aiken, G.R.; Gurtovaya, T.Y. Flux and Age of Dissolved Organic Carbon Exported to the Arctic Ocean: A Carbon Isotopic Study of the Five Largest Arctic Rivers: ARCTIC RIVER DOC. *Global Biogeochemical Cycles* **2007**, *21*, n/a–n/a, doi:10.1029/2007GB002934.
4. Babin, M.; Arrigo, K.; Bélanger, S.; Forget, M.-H.; et al. Ocean Colour Remote Sensing in Polar Seas. *International Ocean Colour Coordinating Group (IOCCG)* **2015**, doi:http://ioccg.org/wp-content/uploads/2015/10/ioccg-report-16.pdf.
5. Matsuoka, A.; Ortega-Retuerta, E.; Bricaud, A.; Arrigo, K.R.; Babin, M. Characteristics of Colored Dissolved Organic Matter (CDOM) in the Western Arctic Ocean: Relationships with Microbial Activities. *Deep Sea Research Part II: Topical Studies in Oceanography* **2015**, *118*, 44–52, doi:10.1016/j.dsr2.2015.02.012.
6. Matsuoka, A.; Huot, Y.; Shimada, K.; Saitoh, S.-I.; Babin, M. Bio-Optical Characteristics of the Western Arctic Ocean: Implications for Ocean Color Algorithms. *Canadian Journal of Remote Sensing* **2007**, *33*, 503–518, doi:10.5589/m07-059.
7. Matsuoka, A.; Bricaud, A.; Benner, R.; Para, J.; Sempéré, R.; Prieur, L.; Bélanger, S.; Babin, M. Tracing the Transport of Colored Dissolved Organic Matter in Water Masses of the Southern Beaufort Sea: Relationship with Hydrographic Characteristics. *Biogeosciences* **2012**, *9*, 925–940, doi:10.5194/bg-9-925-2012.
8. Matsuoka, A.; Hill, V.; Huot, Y.; Babin, M.; Bricaud, A. Seasonal Variability in the Light Absorption Properties of Western Arctic Waters: Parameterization of the Individual Components of Absorption for Ocean Color Applications. *Journal of Geophysical Research: Oceans* **2011**, *116*, doi:10.1029/2009JC005594.

9. Demidov, A.B.; Kopelevich, O.V.; Mosharov, S.A.; Sheberstov, S.V.; Vazyulya, S.V. Modelling Kara Sea Phytoplankton Primary Production: Development and Skill Assessment of Regional Algorithms. *Journal of Sea Research* **2017**, *125*, 1–17, doi:10.1016/j.seares.2017.05.004.
10. Petrenko, D.; Pozdnyakov, D.; Johannessen, J.; Counillon, F.; Sychov, V. Satellite-Derived Multi-Year Trend in Primary Production in the Arctic Ocean. *International Journal of Remote Sensing* **2013**, *34*, 3903–3937, doi:10.1080/01431161.2012.762698.
11. Salyuk, P.A.; Stepochkin, I.E.; Bukin, O.A.; Sokolova, E.B.; Mayor, A.Y.; Shambarova, J.V.; Gorbushkin, A.R. Determination of the Chlorophyll a Concentration by MODIS-Aqua and VIIRS Satellite Radiometers in Eastern Arctic and Bering Sea. *Izvestiya, Atmospheric and Oceanic Physics* **2016**, *52*, 988–998, doi:10.1134/S0001433816090206.
12. Vörösmarty, C.J.; Fekete, B.M.; Meybeck, M.; Lammers, R.B. Global System of Rivers: Its Role in Organizing Continental Land Mass and Defining Land-to-Ocean Linkages. *Global Biogeochemical Cycles* **2000**, *14*, 599–621, doi:10.1029/1999GB900092.
13. Field, C.B.; Behrenfeld, M.J.; Randerson, J.T.; Falkowski, P. Primary Production of the Biosphere: Integrating Terrestrial and Oceanic Components. *Science* **1998**, *281*, 237–240, doi:10.1126/science.281.5374.237.
14. Winder, M.; Sommer, U. Phytoplankton Response to a Changing Climate. *Hydrobiologia* **2012**, *698*, 5–16, doi:10.1007/s10750-012-1149-2.
15. Arrigo, K.R.; van Dijken, G.; Pabi, S. Impact of a Shrinking Arctic Ice Cover on Marine Primary Production. *Geophysical Research Letters* **2008**, *35*, L19603, doi:10.1029/2008GL035028.
16. Bélanger, S.; Babin, M.; Tremblay, J.-É. Increasing Cloudiness in Arctic Damps the Increase in Phytoplankton Primary Production Due to Sea Ice Receding. *Biogeosciences (Online)* **2013**, *10*, 4087–4101, doi:10.5194/bg-10-4087-2013.
17. Kahru, M.; Brotas, V.; Manzano-Sarabia, M.; Mitchell, B.G. Are Phytoplankton Blooms Occurring Earlier in the Arctic? *Global Change Biology* **2011**, *17*, 1733–1739, doi:10.1111/j.1365-2486.2010.02312.x.
18. Lewis, K.M.; Arrigo, K.R. Ocean Color Algorithms for Estimating Chlorophyll a, CDOM Absorption, and Particle Backscattering in the Arctic Ocean. *Journal of Geophysical Research: Oceans* **2020**, *125*, e2019JC015706, doi:10.1029/2019JC015706.
19. Cota, G.F.; Wang, J.; Comiso, J.C. Transformation of Global Satellite Chlorophyll Retrievals with a Regionally Tuned Algorithm. *Remote Sensing of Environment* **2004**, *90*, 373–377, doi:10.1016/j.rse.2004.01.005.
20. Bricaud, A.; Morel, A.; Prieur, L. Absorption by Dissolved Organic Matter of the Sea (Yellow Substance) in the UV and Visible Domains1. *Limnology and Oceanography* **1981**, *26*, 43–53, doi:10.4319/lo.1981.26.1.0043.
21. O'Reilly, J.E.; Maritorena, S.; Mitchell, B.G.; Siegel, D.A.; Carder, K.L.; Garver, S.A.; Kahru, M.; McClain, C. Ocean Color Chlorophyll Algorithms for SeaWiFS. *Journal of Geophysical Research: Oceans* **1998**, *103*, 24937–24953, doi:10.1029/98JC02160.
22. O'Reilly, J.E.; Maritorena, S.; Siegel, D.A.; O'Brien, M.C.; Toole, D.; Mitchell, B.G.; Kahru, M.; Chavez, F.P.; Strutton, P.; Cota, G.F.; et al. Ocean Color Chlorophyll a Algorithms for SeaWiFS, OC2 and OC4: Version 4. *Journal of Geophysical Research: Oceans* **2000**, *103*, 15, doi:10.1029/98JC02160.
23. Wang, J.; Cota, G.F. Remote-Sensing Reflectance in the Beaufort and Chukchi Seas: Observations and Models. *Applied Optics* **2003**, *42*, 2754, doi:10.1364/AO.42.002754.
24. Maritorena, S.; Siegel, D.A.; Peterson, A.R. Optimization of a Semianalytical Ocean Color Model for Global-Scale Applications. *Applied Optics* **2002**, *41*, 2705, doi:10.1364/AO.41.002705.
25. Massicotte, P.; Amon, R.M.W.; Antoine, D.; Archambault, P.; Balzano, S.; Bélanger, S.; Benner, R.; Boeuf, D.; Bricaud, A.; Bruyant, F.; et al. The MALINA Oceanographic Expedition: How Do Changes in Ice Cover, Permafrost and UV Radiation Impact Biodiversity and Biogeochemical Fluxes in the Arctic Ocean? *Earth System Science Data* **2021**, *13*, 1561–1592, doi:10.5194/essd-13-1561-2021.
26. Arrigo, K.R. Impacts of Climate on EcoSystems and Chemistry of the Arctic Pacific Environment (ICESCAPE). *Deep Sea Research Part II: Topical Studies in Oceanography* **2015**, *118*, 1–6, doi:10.1016/j.dsr2.2015.06.007.
27. Sunagawa, S.; Acinas, S.G.; Bork, P.; Bowler, C.; Eveillard, D.; Gorsky, G.; Guidi, L.; Iudicone, D.; Karsenti, E.; Lombard, F.; et al. Tara Oceans: Towards Global Ocean Ecosystems Biology. *Nature Reviews Microbiology* **2020**, *18*, 428–445, doi:10.1038/s41579-020-0364-5.
28. Massicotte, P.; Amiraux, R.; Amyot, M.-P.; Archambault, P.; Ardyna, M.; Arnaud, L.; Artigue, L.; Aubry, C.; Ayotte, P.; Bécu, G.; et al. Green Edge Ice Camp Campaigns: Understanding the Processes Controlling the Under-Ice Arctic Phytoplankton Spring Bloom. *Earth System Science Data* **2020**, *12*, 151–176, doi:10.5194/essd-12-151-2020.
29. Hooker, S.B.; Morrow, J.H.; Matsuoka, A. Apparent Optical Properties of the Canadian Beaufort Sea Part 2: The 1% and 1 Cm Perspective in Deriving and Validating AOP Data Products. *Biogeosciences* **2013**, *10*, 4511–4527, doi:10.5194/bg-10-4511-2013.

30. Antoine, D.; Hooker, S.; Bélanger, S.; Matsuoka, A.; Babin, M. Apparent Optical Properties of the Canadian Beaufort Sea 1: Observational Overview and Water Column Relationships. *Biogeosciences (Online)* **2013**, *10*, 4493–4509, doi:10.5194/bg-10-4493-2013.
31. Van Heukelem, L.; Thomas, C.S. Computer-Assisted High-Performance Liquid Chromatography Method Development with Applications to the Isolation and Analysis of Phytoplankton Pigments. *Journal of Chromatography A* **2001**, *910*, 31–49, doi:10.1016/S0378-4347(00)00603-4.
32. Ras, J.; Claustre, H.; Uitz, J. Spatial Variability of Phytoplankton Pigment Distributions in the Subtropical South Pacific Ocean: Comparison Between in Situ and Predicted Data. *Biogeosciences* **2008**, *5*, 353–369, doi:10.5194/bg-5-353-2008.
33. Hooker, S.B.; Zibordi, G. Platform Perturbations in Above-Water Radiometry. *Applied Optics* **2005**, *44*, 553, doi:10.1364/AO.44.000553.
34. Reynolds, R.A.; Stramski, D.; Neukermans, G. Optical Backscattering by Particles in Arctic Seawater and Relationships to Particle Mass Concentration, Size Distribution, and Bulk Composition: Particle Backscattering in Arctic Seawater. *Limnology and Oceanography* **2016**, *61*, 1869–1890, doi:10.1002/lno.10341.
35. Bricaud, A.; Babin, M.; Claustre, H.; Ras, J.; Tièche, F. Light Absorption Properties and Absorption Budget of Southeast Pacific Waters. *Journal of Geophysical Research* **2010**, *115*, C08009, doi:10.1029/2009JC005517.
36. Lee, Y.J.; Matrai, P.A.; Friedrichs, M.A.M.; Saba, V.S.; Ardyna, M.; Babin, M.; Gosselin, M.; Hirawake, T.; Kang, S.-H.; Lee, S.H. Water Temperature, Primary Productivity-Phytoplankton, Chlorophyll-a Concentration, and Other Data Collected by CTD, Scintillation Counter, Fluorometer, and Other Instruments from Arctic Ocean from 1959-08-03 to 2011-10-21 (NCEI Accession 0161176) 2018.
37. Matsuoka, A.; Hooker, S.B.; Bricaud, A.; Gentili, B.; Babin, M. Estimating Absorption Coefficients of Colored Dissolved Organic Matter (CDOM) Using a Semi-Analytical Algorithm for Southern Beaufort Sea Waters: Application to Deriving Concentrations of Dissolved Organic Carbon from Space. *Biogeosciences* **2013**, *10*, 917–927, doi:10.5194/bg-10-917-2013.
38. Jackson, T.; Grant, M. Ocean Colour Algorithm Blending 2016.
39. Lewis, K.; Van Dijken, G.; Arrigo, K. Bio-Optical Database of the Arctic Ocean 2020, 63356799 bytes.
40. Garver, S.A.; Siegel, D.A. Inherent Optical Property Inversion of Ocean Color Spectra and Its Biogeochemical Interpretation: 1. Time Series from the Sargasso Sea. *Journal of Geophysical Research: Oceans* **1997**, *102*, 18607–18625, doi:10.1029/96JC03243.
41. Seegers, B.N.; Stumpf, R.P.; Schaeffer, B.A.; Loftin, K.A.; Werdell, P.J. Performance Metrics for the Assessment of Satellite Data Products: An Ocean Color Case Study. *Optics Express* **2018**, *26*, 7404, doi:10.1364/OE.26.007404.
42. Legendre, P. Model II Regression User's Guide, r Edition. *R Vignette* **1998**, *14*.
43. Pabi, S.; van Dijken, G.L.; Arrigo, K.R. Primary Production in the Arctic Ocean, 1998. *Journal of Geophysical Research* **2008**, *113*, C08005, doi:10.1029/2007JC004578.
44. Perrette, M.; Yool, A.; Quartly, G.D.; Popova, E.E. Near-Ubiquity of Ice-Edge Blooms in the Arctic. *Biogeosciences Discussions* **2010**, *7*, 8123–8142, doi:10.5194/bgd-7-8123-2010.
45. Ardyna, M.; Babin, M.; Gosselin, M.; Devred, E.; Bélanger, S.; Matsuoka, A.; Tremblay, J.-É. Parameterization of Vertical Chlorophyll a in the Arctic Ocean: Impact of the Subsurface Chlorophyll Maximum on Regional, Seasonal, and Annual Primary Production Estimates. *Biogeosciences (Online)* **2013**, *10*, 4383–4404, doi:10.5194/bg-10-4383-2013.
46. Platt, T.; Gallegos, C.L. Modelling Primary Production. *Springer* **1980**, 339–362, doi:10.1007/978-1-4684-3890-1_19.
47. Morel, A. Available Usable and Stored Radiant Energy in Relation to Marine Photosynthesis. *Deep Sea Research* **1978**, *25*, 673–688, doi:10.1016/0146-6291(78)90623-9.
48. Hessen, D.O.; Carroll, J.; Kjeldstad, B.; Korosov, A.A.; Pettersson, L.H.; Pozdnyakov, D.; Sørensen, K. Input of Organic Carbon as Determinant of Nutrient Fluxes, Light Climate and Productivity in the Ob and Yenisey Estuaries. *Estuarine, Coastal and Shelf Science* **2010**, *88*, 53–62, doi:10.1016/j.ecss.2010.03.006.
49. Wang, J.; Cota, G.F.; Ruble, D.A. Absorption and Backscattering in the Beaufort and Chukchi Seas. *Journal of Geophysical Research* **2005**, *110*, C04014, doi:10.1029/2002JC001653.
50. Bélanger, S.; Babin, M.; Larouche, P. An Empirical Ocean Color Algorithm for Estimating the Contribution of Chromophoric Dissolved Organic Matter to Total Light Absorption in Optically Complex Waters. *Journal of Geophysical Research* **2008**, *113*, C04027, doi:10.1029/2007JC004436.
51. Mustapha, S.B.; Bélanger, S.; Larouche, P. Evaluation of Ocean Color Algorithms in the Southeastern Beaufort Sea, Canadian Arctic: New Parameterization Using SeaWiFS, MODIS, and MERIS Spectral Bands. *Canadian Journal of Remote Sensing* **2012**, *38*, 535–556, doi:10.5589/m12-045.
52. Lewis, K.M.; Mitchell, B.G.; van Dijken, G.L.; Arrigo, K.R. Regional Chlorophyll a Algorithms in the Arctic Ocean and Their Effect on Satellite-Derived Primary Production Estimates. *Deep Sea Research Part II: Topical Studies in Oceanography* **2016**, *130*, 14–27, doi:10.1016/j.dsr2.2016.04.020.

 doi:10.20944/preprints202312.1775.v1